

SPDM: light microscopy with single-molecule resolution at the nanoscale

P. Lemmer · M. Gunkel · D. Baddeley · R. Kaufmann ·
A. Urich · Y. Weiland · J. Reymann · P. Müller ·
M. Hausmann · C. Cremer

Received: 8 June 2008
© Springer-Verlag 2008

Abstract Far-field fluorescence techniques based on the precise determination of object positions have the potential to circumvent the optical resolution limit of direct imaging given by diffraction theory. In order to use localization to obtain structural information far below the diffraction limit, the ‘point-like’ components of the structure have to be detected independently, even if their distance is lower than the conventional optical resolution limit. This goal can be achieved by exploiting various photo-physical properties of the fluorescence labeling (‘spectral signatures’). In first experiments, spectral precision distance microscopy/spectral

position determination microscopy (SPDM) was limited to a relatively small number of components to be resolved within the observation volume. Recently, the introduction of photo-convertible molecules has dramatically increased the number of components which can be independently localized. Here, we present an extension of the SPDM concept, exploiting the novel spectral signature offered by reversible photobleaching of fluorescent proteins. In combination with spatially modulated illumination (SMI) microscopy, at the present stage, we have achieved an estimated effective optical resolution of approximately 20 nm in the lateral and 50 nm in the axial direction, or about 1/25th–1/10th of the exciting wavelength.

P. Lemmer · M. Gunkel · R. Kaufmann · A. Urich · Y. Weiland ·
C. Cremer (✉)
Applied Optics and Information Processing, Kirchhoff Institute
for Physics, University of Heidelberg, Heidelberg, Germany
e-mail: cremer@kip.uni-heidelberg.de
Fax: +49-6221-549112

C. Cremer
Institute for Pharmacy and Molecular Biotechnology
(IPMB)/Bioquant Centre, University of Heidelberg, Heidelberg,
Germany

C. Cremer
Institute for Molecular Biophysics, The Jackson Laboratory,
Bar Harbor, USA

D. Baddeley
Department of Physiology, Faculty of Medical and Health
Sciences, University of Auckland, Auckland, New Zealand

J. Reymann
Bioquant Centre, ViroQuant-CellNetworks RNAi Screening
Facility, University of Heidelberg, Heidelberg, Germany

P. Müller · M. Hausmann
Computer Engineering, Kirchhoff Institute for Physics, University
of Heidelberg, Heidelberg, Germany

PACS 87.64.-t · 87.64.kv · 87.64.M- · 87.80.-y · 87.80.Nj

1 Introduction

While electron microscopy and other ultra-structure imaging methods based on ionizing radiation have the great advantage of an unprecedented resolution, ‘visible’ light (range from near ultraviolet to near infrared) offers other advantages, such as identification of multiple types of appropriately labeled molecules in single, three-dimensionally (3D) intact cells, and even in living ones. Thus, it should be highly useful to complement the potential of ionizing radiation imaging procedures for the study of biological nanostructures with novel approaches to perform high-resolution microscopy using visible light. Potential applications of this are in examining the nanostructure of cell membranes or the genome nanostructures of the cell nucleus [1].

For example, fluorescence resonance energy transfer (FRET) microscopy allows distance measurements between two molecule types down to the few-nanometer level, using

visible light for excitation [2]; fluorescence correlation spectroscopy (FCS) or fluorescence recovery after photobleaching (FRAP) [3] make the analysis of intracellular mobilities of labeled molecules possible. For a full understanding of functional cellular processes, however, additional structural information is necessary. To solve these and many other important problems of cell biology and cellular biophysics, appropriate spatial analysis is indispensable. A serious problem in achieving this goal is that conventional light optical resolution is limited to about 200 nm laterally and 600 nm axially, meaning that cellular nanostructures cannot be adequately resolved to provide full functional information.

Various recently introduced laser-optical ‘nanoscopy’ approaches permit to overcome this problem, and to extend the spatial analysis far beyond the ‘Abbe/Rayleigh limit’ of optical resolution (here assumed to correspond in the object plane (x, y) to about half the wavelength used, according to the original formulas, and to about one wavelength in the direction of the optical axis (z)).

For example, in the concept of confocal laser scanning fluorescence 4Pi microscopy the object is scanned by laser light focused from different sides (‘4Pi’ geometry) and the fluorescence excited is detected ‘point-by-point’ [4]. Using two opposing high numerical aperture lenses to concentrate two coherent opposing laser beams in a joint focus, confocal laser scanning 4Pi microscopy [5–9] has become an established ‘nanoscopy’ method, allowing an axial optical resolution down to the 100-nm range. Compared to the results of conventional fluorescence microscopy methods, this resolution is 5–7 times better.

In many imaging applications, the structural information desired is the size of nanostructures which are separated from each other by a distance larger than the Abbe limit. To solve this problem, spatially modulated illumination (SMI) far field light microscopy [10–13] is one of the many possibilities for using structured illumination [14, 53–55] to improve spatial analysis. SMI microscopy is based on the creation of a standing wave field of laser light, which can be realized in various ways, such as by focusing coherent light into the back focal planes of two opposing objective lenses. The fluorescently labeled object is placed between the two lenses and moved axially in small steps (e.g. 20 nm or 40 nm) through the standing wave field. At each step, the emitted fluorescence is registered by a highly sensitive CCD camera. This procedure allowed axial diameter measurements of individual fluorescent subwavelength-sized objects down to a few tens of nm, and also the determination of axial distances between ‘point-like’ fluorescent objects (at lateral distances larger than the Abbe limit) down to the range of a few tens of nm and with a precision in the 1-nm range. Several biophysical application examples indicate the usefulness of SMI ‘nanoscopy’ for the study of the size of transcription factories [15] and of individual gene regions [16, 17].

Stimulated emission depletion (STED) microscopy [18] is a focused beam method, in which the size of the excited region is greatly reduced by stimulated emission depletion [19]. Presently, this technique allows an optical lateral (x, y) resolution in the 15–20 nm range using visible light. In cases where the field of view can be made sufficiently small (in the few-micrometer range), in vivo STED microscopy with tens of frames/s has been reported. STED microscopy can be regarded as a special case of RESOLFT (reversible saturable optical fluorescence transition microscopy) where, in principle, optical resolution in the few-nm range should become possible using visible light [20].

In this report, we shall describe an complementary approach in achieving molecular resolution using spectral precision distance microscopy/spectral position determination microscopy (SPDM).

SPDM [21–24] is a far-field fluorescence light microscopy method based on (a) labeling of neighboring ‘point-like’ objects with different spectral signatures (for abbreviation also called ‘colors’), where ‘different spectral signatures’ were realized originally by different excitation/emission spectra, but were conceived to include also other ‘photon-sorting’ modes like fluorescence lifetimes, photoluminescence and stochastic labeling schemes [25] to allow photophysical discrimination; (b) spectrally selective registration to ‘sort’ the emitted photons according to their spectral signature; (c) high-precision position monitoring. In combination with fluorescence lifetime measurements, the application of the SPDM concept to nanometer resolution of single molecules was experimentally confirmed [26]. Since the original reports [21–29] a number of conceptually related far-field fluorescence methods have been described, like FPALM, PALM, PALMIRA, STORM, etc. [30–35]. As a general denomination, all these approaches might be regarded as methods of ‘spectrally assigned localization microscopy’ (SALM), where the localization of an object is assigned due to a characteristic spectral signature. The basic condition of SPDM/SALM is ‘optical isolation’ [27, 28]. This means that in a given diffraction-limited observation volume defined for example by the (x, y, z) full-width-at-half-maximum (FWHM) of the point spread function (PSF) of the microscope system used, at a given time interval and for a given spectral registration mode, only one such object (e.g. a single molecule) is registered (under certain conditions there may be a few [25]). During the first experimental applications of SPDM to biological nanostructure elucidation [29, 36], the objects were labeled with fluorochrome molecules which had different emission wavelengths, and the signals were acquired synchronously. However, fluorescence emission spectra of selectable molecules with typically 50-nm bandwidth are relatively broad. As such, in fluorescence microscopy, the detectable wavelengths are limited to a complete range of about 600 nm, and

only a few ‘colors’ (in the sense of variation in the emission spectra) can be used at the same time within the same object.

To overcome this restriction, different methods of ‘optical object isolation’ in the time domain are currently used. One possibility to overcome this is ‘photoactivated localization microscopy’ [30, 31]. Molecules and proteins that are used for this method are fluorescent markers which are chemically modified (e.g. by adding appropriate side groups) in such a way that most of them are initially in an inactive state for the fluorescence excitation at a given wavelength λ_{exc} . This state (i.e. a ‘dark’ spectral signature with respect to a wavelength $\lambda_{\text{fl}1}$) can be changed to a fluorescent one (i.e. a ‘bright’ spectral signature with respect to a wavelength $\lambda_{\text{fl}2}$), for example by illumination with light of a defined wavelength λ_{act} (e.g. in the near ultraviolet) which is different from the one of fluorescence excitation. If the activation of the fluorescent markers (i.e. transition from a ‘dark’ spectral signature to a ‘bright’ one) is done stochastically by using low intensities, only a few molecules within one acquisition time interval of the detector are activated, and thus the optical isolation of their signal can be achieved. Due to subsequent illumination with λ_{exc} , the fluorescent signal emitted by these optically isolated molecules (‘bright’ spectral signature) is then registered until they are irreversibly bleached (i.e. irreversible transition to a ‘dark’ spectral signature). From these fluorescent signals, the positions of the corresponding molecules can be determined with high precision. Under good optical conditions, a localization accuracy in the few-nm range is possible. Repetition of this procedure (e.g. by registration of 10 000 individual image frames) allows to obtain the positions of the individual molecules even if their mutual distances are far below the Abbe/Rayleigh limit. The photoactivation process at λ_{act} and the use of a second laser line (λ_{exc}) can be avoided if an auto-activation of the molecules by the read-out laser (λ_{exc}) is used [33]. Instead of irreversible bleaching, reversible photoswitching between a ‘dark’ and a ‘bright’ spectral signature can also be used to achieve optical isolation [32, 34].

Another possibility to obtain the optical isolation required may be reversible photobleaching [38]. Unlike the usual bleaching effect used in PALM [30] or FPALM [31], where the structure of fluorescent molecules is irreversibly modified towards a non-fluorescent ‘dark’ spectral signature state (at given excitation/emission conditions), this effect is a reversible one. The functional connection between the three fundamental states of a molecule under these latter conditions may be described with the transitions $M_{\text{rbl}} \xrightleftharpoons[k_1]{k_2} M_{\text{fl}} \xrightarrow{k_3} M_{\text{ibl}}$, wherein M_{rbl} is the reversibly bleached state, M_{fl} is the fluorescent state and M_{ibl} is the irreversibly bleached state. The rate constants of the cross-

ing processes are indicated with k_i ($i = 1, 2, 3$), where the processes are assumed to be first-order reactions. The ratio between the probabilities for reversible and irreversible bleaching $P_{\text{rbl}}/P_{\text{ibl}}$ can be significantly affected by physicochemical modifications of the molecule due to its environment, or due to illumination with light of appropriate wavelength (‘physicochemically modified fluorophores’). This effect was well studied in the context of fluorescent protein derivatives from the jellyfish *Aequorea victoria* [38–42]. After starting to illuminate fluorescent molecules (M_{fl}) with excitation light, a certain amount (dependent on P_{rbl}) is bleached instantly ($M_{\text{fl}} \xrightarrow{k_3} M_{\text{ibl}}$). Another amount is transferred into the reversible dark state ($M_{\text{fl}} \xrightarrow{k_2} M_{\text{rbl}}$). We envisaged that the statistical recovery of fluorescent molecules (‘bright’ spectral signature) from this state (M_{rbl}) and transition into an irreversibly bleached state of a ‘dark’ spectral signature (M_{ibl}), with a delay time sufficient for single fluorescent molecule registration, would allow an additional possibility for optical isolation of single molecules in the time domain. This would offer another approach to high-resolution SPDM/SALM of the number and positions of molecules (even of the same type) within a given observation volume.

To realize this, the condition has to be provided that within the integration time of the detector, the density of molecules with a ‘bright’ spectral signature (M_{fl}) should not be higher than statistically one fluorescent molecule per diffraction limited observation volume (given by the three-dimensional PSF). Fast recovery and bleaching rates have to be established since acquisition time is a very critical factor in localization microscopy, due to the up to thousands of single image frames which may be required for a highly resolved SPDM/SALM image consisting of a large number of localized molecules. To accelerate the read-out and bleaching times, light of high intensity may have to be used. The final image of the object is obtained when the positions of all the localized molecules are copied into a joint SPDM image space.

Although in various SALM methods the lateral (x, y) localization of single molecules (object plane perpendicular to the optical axis) has been firmly established, the localization (z) along the optical axis has proved to be challenging. To obtain 3D reconstructions of the labeled objects (i.e. the x, y, z coordinates of the fluorescently labeled molecules), various approaches have been applied. One solution is to use confocal laser scanning or confocal laser scanning 4Pi microscopy [29, 36, 37, 43] to obtain the 3D positions of the objects.

Another possibility is to use the 3D information within the laterally acquired signal. Since all light-emitting molecules are ‘point like’, one can assume that they all are imaged in the same way (disregarding spatial orientation effects of the molecules as producing aberrations in the few-

nm range under the conditions used [44]). The fact that out-of-focus objects appear more blurred, and that the PSF is not symmetric along the optical axis [45], can be used to localize photon-emitting sources in all spatial dimensions. If the propagation path of the electromagnetic waves is well known, under otherwise ideal registration conditions the accuracy of the axial localization (z) is restricted only by the number of the photons detected [25, 50], analogous to lateral localization (x, y) [28]. Using common photoactivatable or photoswitchable fluorophores in combination with biplane detection [46], or a systematically modified detection PSF [34], a 3D localization accuracy of about 50–80 nm FWHM was recently achieved.

SPDM in combination with spatially modulated illumination (SMI) along the optical axis is a further method for use in performing 3D single-molecule localization and corresponding 3D effective optical resolution. SMI microscopy allows the determination of the axial extension ('size') of a fluorescently labeled nanostructure (at a given x, y position) down to a minimum of a few tens of nm [12, 13, 47]. For example, if the axial (z) extension dz of such a nanostructure has been determined to be 30 nm, this means that most of the molecules within this nanostructure have an axial distance from each other not exceeding 30 nm [11]. Consequently, the smallest resolvable axial distance (or z -resolution) would also be around 30 nm; if a significant number of molecules would have a larger z -distance from each other, this would lead to a broader axial (z) extension than measured. In addition, the mean axial localization z_0 of these molecules is corresponding to the relative position of the axial SMI intensity distribution. From this general idea, the following measuring approach was envisaged. Firstly, the localization z_0 and the position interval dz of the molecules around z_0 and along the optical axis (z) are determined for every single (x, y) pixel.

The smaller the axial extensions dz of the labeled nanostructures are, the more precisely their markers (fluorescent molecules) can be localized around z_0 and along the optical axis, and hence the better the axial effective optical resolution will be (i.e. the smallest axial distance between two labeled molecules which can be detected). For example, if the lateral (x, y) localization accuracy is assumed to be 15 nm, and if the minimum measurable axial (z) extension dz is assumed to be 30 nm, then a lateral distance between molecules equal to or larger than about 35 nm should be detectable; in the axial direction, if fluorescent molecules would have a distance larger than 30 nm, this should be detectable due the resulting broadening of the axial extension. From this, for this example an overall 3D resolution of around 40 nm may be estimated.

2 Methods

2.1 Optical setup

To perform SPDM experiments with molecules subjected to reversible photobleaching, we used an SMI microscope setup (Fig. 1). For illumination, up to three laser sources are available for $\lambda_{\text{exc}} = 488 \text{ nm}$, 568 nm and 647 nm (Lexel 95-4, Lexel 95L-K and Lexel 95-K, Lexel Laser, USA) excitation, which can be independently switched on and off with shutters before being combined with dichroic mirrors (AHF Analysentechnik AG, Tübingen, Germany). The three laser lines are directed into the collimator, consisting of two achromates (Linos Photonics, Göttingen, Germany) with 10 mm and 100 mm focal lengths, respectively, to expand the beam to a diameter of approximately 20 mm. The expanded laser beam is then split by a 50 : 50 beam splitter (BS) (Edmund Optics, Karlsruhe, Germany), yielding two coherent counterpropagating and collimated laser beams which are focused into the back focal plane of two opposing oil immersion objective lenses (Obj. 1 and Obj. 2) ($\times 100$, NA = 1.4, Leica, Bensheim, Germany). This results in two counterpropagating collimated laser beams. Interference between these two beams produces a standing wave field in the space between the two objective lenses, and hence a \cos^2 -shape distribution of the intensity along the optical axis (z).

Samples may be prepared using ordinary object slides (and/or cover slips) and are then placed between the two objective lenses and moved along the optical axis with a piezoelectrical stage (Physik Instrumente, Karlsruhe, Germany),

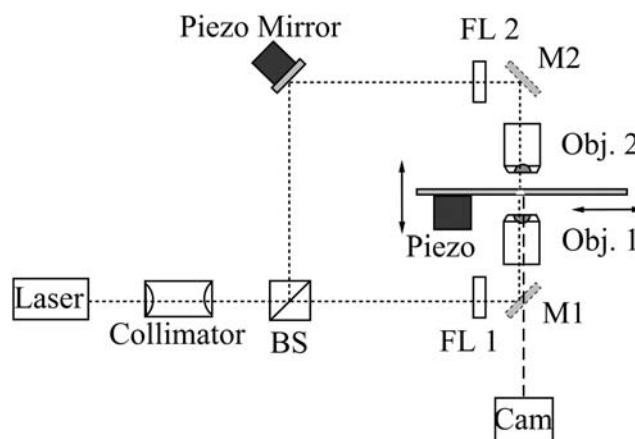


Fig. 1 A schematic overview of the SMI setup used for the SPDM experiments. The major improvement compared to a wide-field fluorescence microscope is the structured illumination pattern in the form of a standing wave field along the optical axis created between the two objective lenses. This standing wave field permits accurate axial size and position information to be obtained. A second detection path using the second objective and a further sensor can easily be established, allowing either the detected photon number to be doubled, or biplanar detection to be implemented whilst retaining the same in-plane signal strength

allowing 3D image stacks of the specimens to be recorded. An additional piezo-electrical stage controlling the position of a mounted mirror (Piezo Mirror) allows the relative phase in the two interferometer arms to be varied in a controlled way. The emission light from the fluorescently labeled target regions, collected by the detection objective lens (Obj. 1), is then separated from the excitation light by a dichroic mirror (D1) (AHF Analysentechnik AG, Tübingen, Germany) and focused by a tube lens ($\times 1.0$, Leica, Bensheim, Germany) onto a highly sensitive 12-bit black-and-white CCD camera (CCD, SensiCam QE, PCO Imaging, Kelheim, Germany) for imaging. In front of the CCD chip, a blocking filter (BF) in a filter wheel blocks any remaining excitation light and, depending on filter selection, out-of-band fluorescence. Moreover, a white light emitting diode can be used in transmission mode to locate the focal plane in order to reduce bleaching of the dyes.

2.2 Data acquisition

The combination of SPDM/SMI methods for high-resolution 3D imaging described here depends on the use of two different acquisition processes, a SPDM localization image and SMI analysis. First, SMI images were taken at low illumination intensities with negligible bleaching (typical intensity of about 100 W/cm^2 and camera integration time of 100 ms per frame). For this, object and structured illumination were moved relative to each other in discrete steps (Δz) of typically 20–40 nm. In case the object was stationary and the structured illumination was moved (by adjusting the piezo mirror in Fig. 1), this was called a phase scan. Otherwise, if the object itself was moved in the standing wave field (by adjusting the piezo stage in Fig. 1), the process was called an object scan. Each of these methods was found to allow us to yield the desired axial information. After each scan step a wide-field image was recorded by the CCD camera, and all the images (about 200 for each object) were saved within a data stack.

After the SMI mode registration was completed, data acquisition for the two-dimensional (2D) SPDM localization was performed at high laser intensities of about 10 kW/cm^2 – 1 MW/cm^2 ; in this report, only one laser line ($\lambda_{\text{exc}} = 488 \text{ nm}$) was used for all measurements. During the 2D SPDM acquisition process the object was situated in the focal plane and no further object movement was necessary. Applying frame rates of 10–18 fps, the individual wide-field images (usually about 1000 to 3000 per object) were saved in sequence within a time stack.

The region of interest was the same for the two acquisition processes, and was usually set in the range of 100 – $5000 \text{ }\mu\text{m}^2$, depending on the structure of interest.

2.3 Evaluation

2D localization

After the data acquisition, the first evaluation step was 2D SPDM localization. It is important to note that the source of the acquired signal was a single ‘point-like’ molecule (i.e. diameter $\ll \lambda_{\text{exc}}$). Hence, for the evaluation the knowledge of how ‘point-like’ objects are imaged by the microscope system was applied. Based on this knowledge, a model function was fitted to the acquired signals, taking into account effects of data sampling (size and distance of pixels) and the corresponding noise nature [28, 31, 48]. To use the noise considerations of the fitting algorithm in an appropriate way, a conversion from camera counts to photons had to be performed. According to the manual of the CCD camera used, in low-light mode the quantum efficiency for yellow fluorescent protein (YFP) emission radiation between 490 and 560 nm is $64 \pm 1\%$ or $0.64 \text{ e}^-/\text{photon}$. Since the analog/digital (A/D) conversion factor in this high-gain mode is $2 \text{ e}^-/\text{count}$, the count number was multiplied by $2/0.64$ photons/count = 3.13 photons/count.

For comparison, the fitting process was done using two different implementations of the Levenburg–Marquardt algorithm [47] with a Gaussian distribution $f(x, y)$ of photons as a model function for the signal in the object plane:

$$f(x, y) = A \exp\left(\frac{(x_0 - x)^2 + (y_0 - y)^2}{2\sigma^2}\right) + B_0 + B_1(x_0 - x) + B_2(y_0 - y).$$

Here, x_0 and y_0 are the starting parameters for the position, which were determined as the center of the segmented signal, A is the amplitude of the distribution and B_0 , B_1 and B_2 are parameters describing a linear background.

The first fitting algorithm was implemented in MatLab (The MathWorks, Inc., www.mathworks.com). This algorithm solves the weighted least squares problem considering the known noise model of the signal acquisition (Gaussian read-out noise of the detector combined with Poissonian photon and conversion noise). The second algorithm is ‘leastsq’, a part of the python (www.python.org) module ‘SciPy.optimize.minpack’ (www.scipy.org). The origin of the signal and, hence, the position of the source molecule can be determined laterally (i.e. in the object plane) with an accuracy (standard deviation) σ_{lat} of less than 5 nm (‘localization accuracy’). Under the conditions used here, localization errors resulting from the unknown orientation of the molecules can be neglected [44]. Since the limit of the localization accuracy can be estimated by the relation $\sigma_{\text{lat}} \sim \lambda_{\text{emission}}/[\text{NA} * n_{\gamma}^{1/2}]$, given the emission wavelength $\lambda_{\text{emission}}$, the numerical aperture of the optics NA and the number of detected photons n_{γ} , the main limitation of localization precision is the number of collected photons [11, 25, 28, 31, 48, 52].

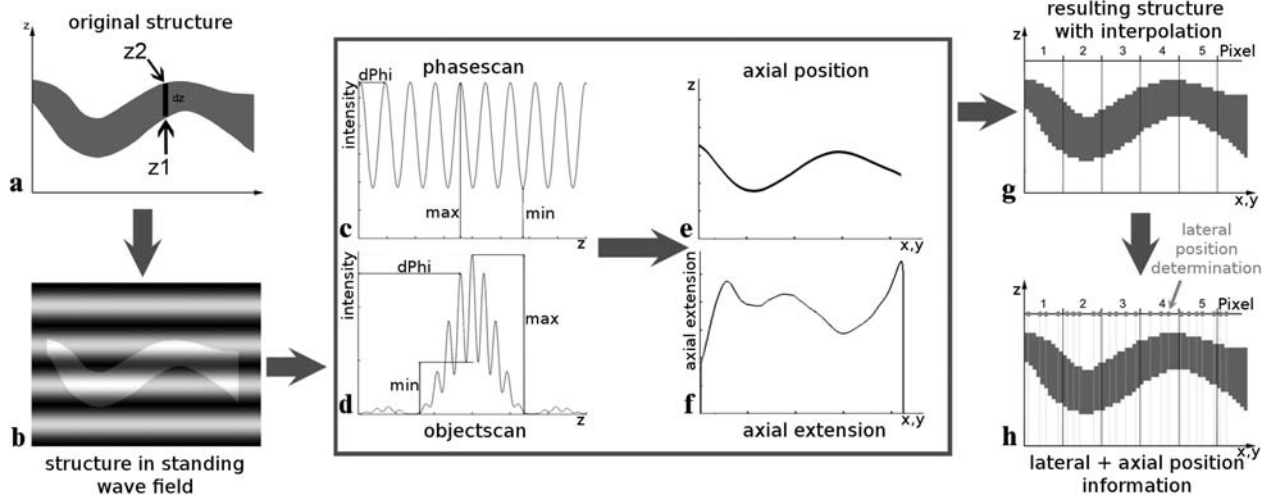


Fig. 2 Scheme of the 3D SPDM/SMI process. The object of interest (a) is placed within a standing wave field along the optical axis (b). By performing a phase scan (c) or an object scan (d), both the relative axial position z_0 (e) and the axial extension dz (f) can be obtained from

the registered data. The interpolated axial information (g) can then be combined with the single-molecule positions of the 2D SPDM localization, resulting in a 3D image with an effective 3D optical resolution at the nanoscale (h).

3D localization

The principle of 3D localization is presented in Fig. 2. An exemplary nanostructure of interest with x , y (lateral) and z (axial) distribution is shown in Fig. 2a. All molecules of the nanostructure at a given x , y position are assumed to have an axial extension of less than approximately 130 nm (for example, $dz \approx 60$ nm). In Fig. 2b, the structure is excited by a standing wave field. Either the standing wave field (phase scan, Fig. 2c) or the object (object scan, Fig. 2d) is moved in equal steps (usually $\Delta z = 20$ – 40 nm). At each step the fluorescence emission is detected and saved separately in one frame. All the frames then are saved into a 3D data stack displaying the axial mean position z_0 (Fig. 2e), which is obtained from the maximum of the SMI intensity distribution in Fig. 2d. Evaluating the scan data (phase scan or object scan data), the spatial extension dz of the object (determined from the contrast in modulation $r = (\max - \min) / \max$, where \max is the maximal intensity and \min the minimal intensity along the time axis (corresponding to the z coordinate) can be obtained with a precision of a few nanometers [10, 11, 13, 47]. In Fig. 2g, the axial (z) data is merged for all pixels of the lateral (x , y) region of interest. After the 2D localization process, the lateral (x , y) positions of the single fluorophores are complemented with the respective axial (z) information, resulting in an SPDM image with, for example, 30 nm lateral effective optical resolution (obtained from the x , y localization measurements) and 40 nm axial effective optical resolution (obtained from the z -extension measurements). If only one fluorophore with sufficient photostability is excited along the z

axis, its z position may be monitored by SMI with an accuracy even in the 1–2 nm range [13].

2.4 Sample preparation

As an application example for using high-resolution 3D SPDM/SMI for imaging of biological nanostructures, the plasma membrane of the human breast cancer cell line Cal-51 was labeled with yellow fluorescent protein (YFP).

Cal-51 (DSMZ, Braunschweig) breast cancer cells of human origin were routinely cultivated in DMEM medium supplemented with 10% FCS, 1% L-glutamine and 1% penicillin/streptomycin at 37°C and 5% CO₂ in a humidified incubator. The cells were then seeded onto 20 mm × 20 mm cover slips and grown overnight at 37°C and 5% CO₂ in a humidified incubator. Labeling of the plasma membrane was performed by Organelle Lights (Invitrogen Corporation, Carlsbad, USA) according to the manufacturer's protocol. The kit is based on genetically encoded fluorescent proteins (YFP) fused to signal peptides that direct the fluorescent markers to specific cellular compartments, in this case the plasma membrane. Cellular delivery was achieved by the BacMam technology, based on the baculovirus. The cells were then incubated for 24 h at 37°C and 5% CO₂ in a humidified incubator and subsequently fixed in 4% formaldehyde in PBS to stabilize the cellular structure. The transduction efficiency was about 60%.

The cells were mounted with ProLongGold antifade reagent (Invitrogen). One drop of antifade reagent was placed onto an object slide and the cover slip, with the cell side down, was carefully lowered onto it. The slides were

sealed with nail polish and stored at 4°C in the dark until usage.

3 Results

3.1 2D SPDM of biological nanostructures

As a first application example, the SPDM extension described above was used for the 2D reconstruction of the distribution of membrane localized fluorescent proteins. Figures 3 and 4 show both conventional wide-field fluorescence images and corresponding two-dimensional SPDM images of such proteins in cellular plasma membrane protrusions. Both images were acquired with the above-described SMI microscope setup. Cells of the human breast cancer cell line Cal-51 were labeled with yellow fluorescent protein (YFP). During the SPDM imaging process, the YFP molecules were subjected to an appropriate physical modification based on reversible photobleaching as described in Sect. 1. In both cases, the connection between a fluorescence-labeled cell

and one without marker proteins is shown. For smoother appearance and to indicate the estimated mean localization precision, the pixels (10-nm pixel size) corresponding to the positions and number of the localized fluorescent proteins were blurred via a Gaussian kernel with 15-nm standard deviation.

It may be noted that the (x, y) width of the finest structures resolved (cellular protrusions) in the SPDM images amounted to about 50–60 nm. The number of collected photons per molecule distribution (Fig. 5) allowed us to estimate the limiting localization accuracy due to photon statistics (see Sect. 2.3) to be in the range of 6 nm; this was compatible with the experimental localization accuracy (Fig. 6) of about 15 nm obtained by the fitting procedure. The total number of localized protein molecules in these examples was 12 691 for the first (Fig. 3) and 6871 for the second Cal-51 cell (Fig. 4), respectively. In both cases, the total data acquisition time was about two and a half minutes while 2000 wide-field images were recorded at an average frame rate of about 13 frames per second. The mean photon numbers per molecule registered were about 1300 for the first and about

Fig. 3 Cellular plasma membrane protrusions (*arrow*) in a human Cal-51 cell expressing membrane-localized YFP. *Large image and insert:* conventional wide-field image. The high dynamic range of the sensitive CCD camera permitted both the labeled cell of interest and its weakly auto-fluorescent neighbor (N) to be visualized. *Right:* high-resolution SPDM image obtained from inset (*left*)

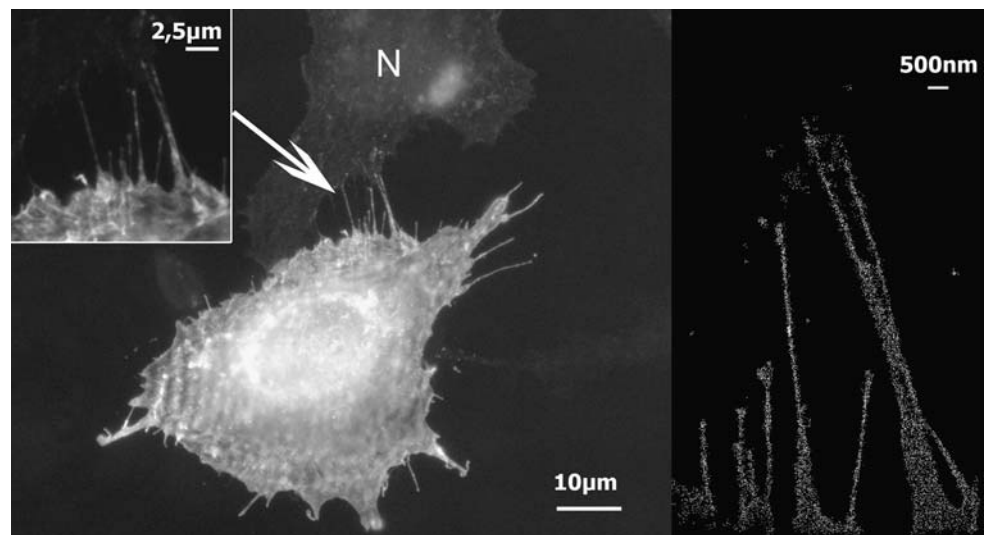
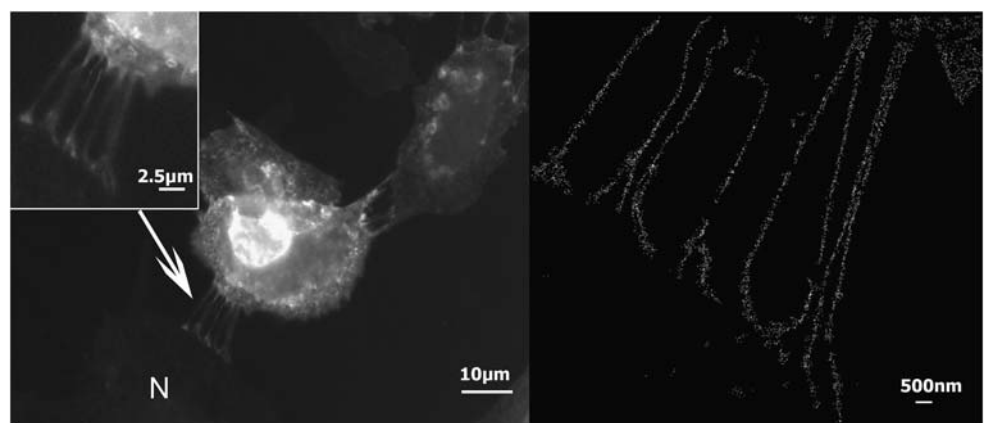


Fig. 4 A second example for SPDM imaging of a Cal-51 cell expressing YFP. In this case, no localization signal was obtained from the untransfected cell (N), confirming that the technique was indeed specific for the fluorescence labeling applied. *Left-hand figures (large image and insert)* show the conventional wide-field fluorescence image. The image at the *right* shows the SPDM image of the wide-field image presented in the inset in the *upper left*



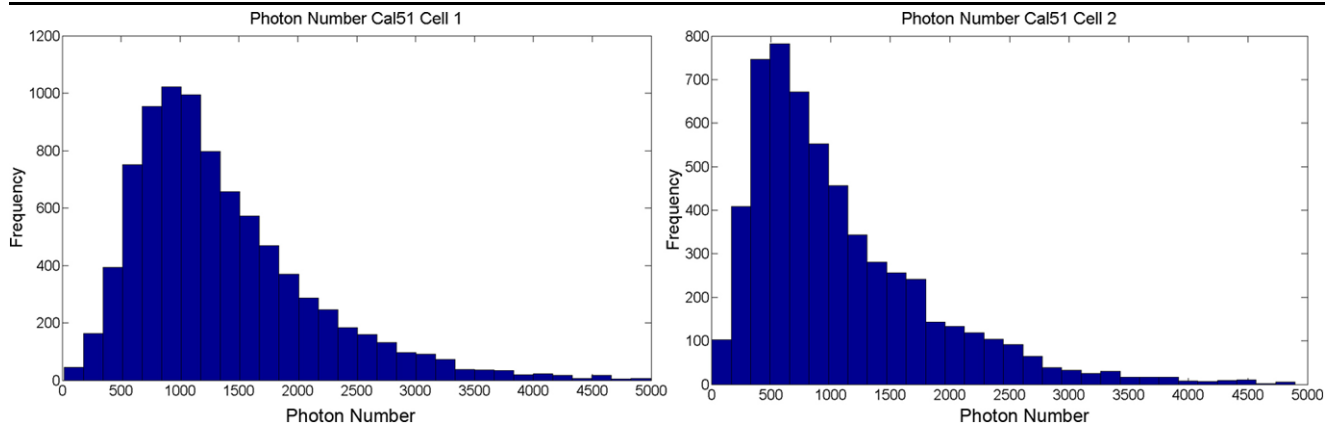


Fig. 5 Histograms of the distributions of photon numbers registered per molecule for the two Cal-51 cells of Figs. 3 (left) and 4 (right). The mean photon numbers estimated were 1361 for the left- and 1080 for the right-hand distribution

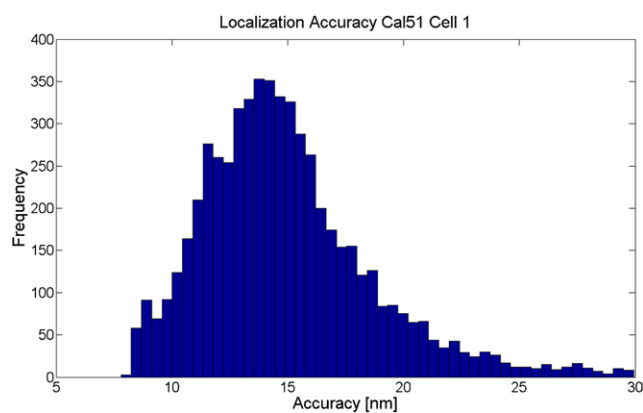


Fig. 6 Histogram of the estimated localization accuracy (pair-wise mean value of x and y localization precision) for the Cal-51 cell in Fig. 3. The overall mean value of the localization precision was 14.9 nm with a standard deviation of 3.9 nm. The total number of localized fluorochromes was 12 691

1100 for the second cell. The fitting procedure took an additional 3 min using python and about 10 min in MatLab on a single core of a conventional PC without the implementation of acceleration methods. The relevant values (photon number, localization accuracy and the number of localized molecules) were very similar throughout the whole series of more than 100 SPDM images, which were acquired from two specimens within a few days.

3.2 3D SPDM of experimental biological nanostructures

As a first example of 3D SPDM/SMI reconstruction, a Cal-51 cell (plasma membrane labeled with physicochemically modified YFP) was first imaged in wide-field mode with spatially modulated illumination (\cos^2 intensity distribution along the optical axis). The epi-fluorescence overview image of the cell is shown in Fig. 7. The standing wave field was then moved through the object space with a step size

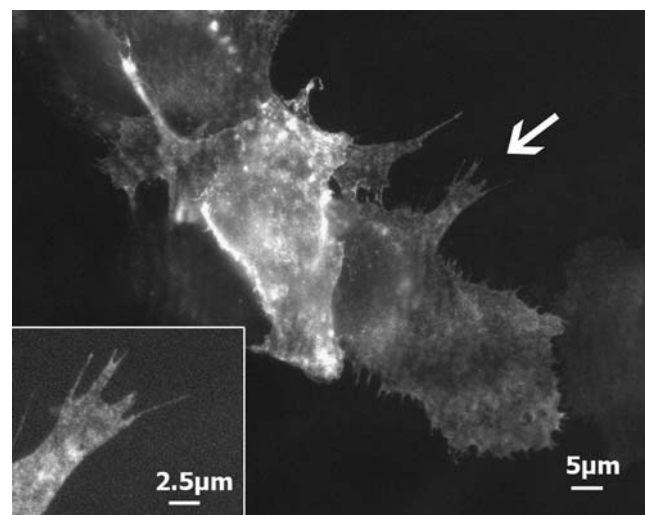


Fig. 7 Overview epi-fluorescence image of the Cal-51 cell used for 3D SPDM. An *arrow* is pointing to the plasma membrane protrusions examined, which are additionally presented in the *lower left corner* with a higher zoom factor

$\Delta z = 25$ nm for 5 μm (phase scan). The emission of the cellular plasma membrane protrusions (see inset in Fig. 7) was recorded for every Δz step. Compared to the experimentally effective wavelength ($\lambda_{\text{exc}}/n \sim 330$ nm) and the accuracy of the z -positioning of the piezo-actuator (4-nm standard deviation), this process corresponds to a large over-sampling. However, since the total acquisition time was about 20 s, there was no need to use larger step sizes or fewer steps.

By performing a single-dimension Fourier transformation along the time axis, and knowing the wavelength of the light pattern (330 nm), the phase was determined for every lateral (x, y) pixel of the stack. To obtain the position of the emission center for every pixel, the phase was shifted by $\pi/2$ and multiplied with the wavelength of the modulated illumination. The result is shown in Fig. 8. To determine the extension dz of the object along the optical axis, the modified

Fig. 8 The (x, y) pixels indicate the mean z position (z_0) of the corresponding object emission center (for conventional wide-field image see *insert* in Fig. 7). To obtain a smooth transition between the single pixels, the image was resized by a bicubic interpolation. The *color bar* indicates the relative z_0 position in nanometers (nm). Higher values indicate nearness to the cover slip to which the cell was attached

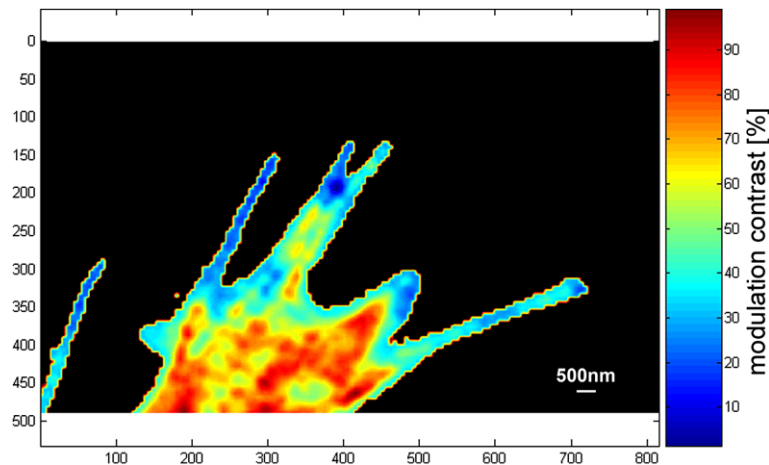
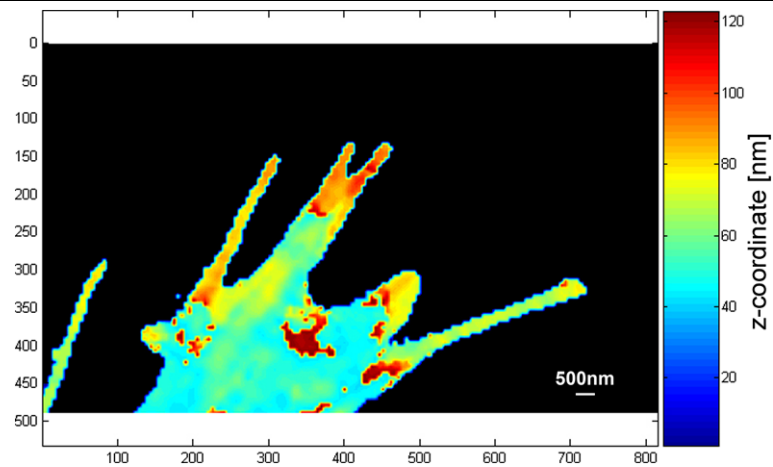


Fig. 9 Each (x, y) pixel represents the axial size of the structure of Fig. 8 along the optical axis (z). Bicubic interpolation of the image was used to obtain smooth transitions between single pixels. The *color bar* indicates the modified modulation contrast ($R_{\text{mod}} = I_{\text{min}}/I_{\text{max}}$) in percent (for I_{min} and I_{max} see Figs. 2c, d). Structure elements with a small axial extension (ϑ) correspond to an object scan intensity

distribution (Fig. 2d) with a low modified modulation contrast (R_{mod}). If the structure is supposed to be tube-like and homogeneously labeled, the following relations may be estimated for a \cos^2 -shaped standing wave field produced with 488-nm excitation light: $R_{\text{mod}} = 10\% \Rightarrow \vartheta \approx 50$ nm, $R_{\text{mod}} = 40\% \Rightarrow \vartheta \approx 140$ nm, $R_{\text{mod}} = 70\% \Rightarrow \vartheta \approx 190$ nm

modulation contrast $R_{\text{mod}} (= I_{\text{min}}/I_{\text{max}}$, see Fig. 2) was calculated from the information stored in the SMI mode images (Fig. 9). Using the Fourier domain, the amplitude and the constant contingent of the modulation were directly determined after adjusting the zero level by subtracting the background. In the next step, the contrast image was correlated with the corresponding structure sizes.

The next step after the analysis of axial positions z_0 and extensions dz was 2D SPDM localization of the single molecules in the same object. Then, the obtained 2D localization image (x, y) data (Fig. 10) was combined with the SMI (z_0) position and size (axial extension dz) information. For the SPDM/SMI 3D reconstruction, only the volume of one plasma membrane protrusion (indicated by an arrow in Fig. 10) was included in the calculations.

The result of the subsequent volume rendering with Voxx (www.nephrology.iupui.edu/imaging/voxx/) is shown

in Fig. 11. As expected from visual inspection of Figs. 9 and 10, the protrusions are very small, both in x, y width (minimum width Δx about 55 nm) and in the z direction (minimum Δz about 50 nm). Hence, the structure of this protrusion is compatible with that of a rod of about 3 μm in length and approx. 50 nm in diameter.

4 Discussion

Various approaches for far-field fluorescence microscopy have been described to overcome the limitations of conventional light microscopy given by the Abbe/Rayleigh limit of optical resolution.

The general idea to use different spectral characteristics of the object to improve nanostructure analysis has been put forward since the beginning of the 1980s [51, 52], based on

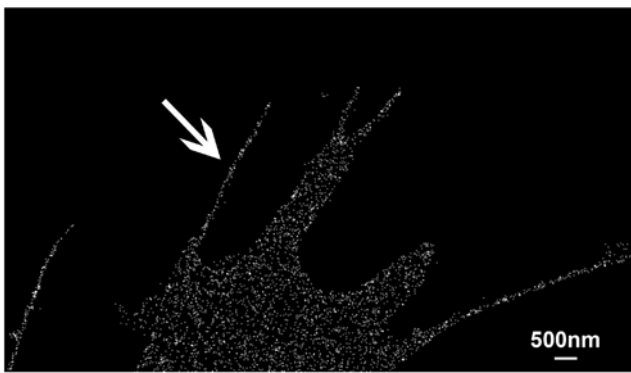


Fig. 10 2D SPDM localization step for SPDM/SMI 3D reconstruction. In total, the (x, y) positions of 4137 single molecules were determined and inserted into the pixel grid, which had an effective pixel size of 5 nm. The pixels with the localized molecules were blurred with a Gaussian kernel (standard deviation 10 nm)

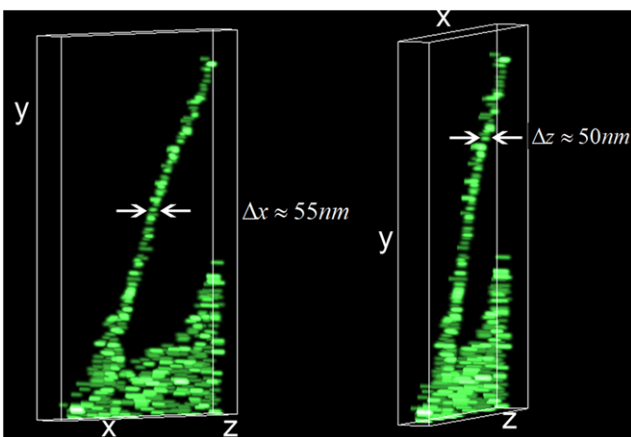


Fig. 11 3D SPDM/SMI reconstruction of a human cancer cell protrusion (see Figs. 9 and 10). The volume rendering results are shown in two different orientations

ideas used earlier in astronomy. However, to our knowledge the extension of such basic concepts to far-field fluorescence microscopy has been initiated only since the mid 1990s.

In this report, an extension of spectral precision distance microscopy/spectral position determination microscopy (SPDM) [27], a method of spectrally assigned localization microscopy (SALM), was presented. This novel extension of SPDM features the use of ‘conventional’ fluorescent proteins, i.e. without the chemical modifications described for PALM and FPALM applications [30, 31]. Since biological specimens labeled with such fluorescent proteins are most common, SPDM methods using such fluorophores have a vast range of applications, including the potential for *in vivo* measurements. The results described here indicate that single molecule (x, y) localization accuracies below 10 nm are possible not only for special photoactivatable fluorescent proteins [30, 31] but also for ‘conventional’ ones. The typical data acquisition time achieved here was about 100 s, in

which an object area of up to $90 \mu\text{m} \times 90 \mu\text{m}$ was recorded and more than 100 000 molecules were localized (Lemmer et al., private communication). Presently, the data processing aspect of molecule localization and object reconstruction still takes time in the order of a few minutes. By using fast modern multi-core processors, calculations could be carried out on-line during image acquisition. Hence, high-throughput fluorescence imaging at molecular optical resolution applying visible light in combination with widely used fluorophores becomes feasible.

In addition, a novel alternative has been presented in this report for fast 3D imaging of biological nanostructures with an effective 3D optical resolution (x, y, z) of single molecules in the range of 50 nm, corresponding to about 1/10th of the exciting wavelength. This has been achieved by a combination of SPDM lateral (x, y) localization microscopy and SMI axial size dz and mean position z_0 determination. For the application of this SPDM/SMI 3D imaging approach, some a priori information about the labeled object is required. This condition however can be fulfilled for most biological nanostructures to be analyzed. As an example, membrane-associated proteins were used to elucidate the 3D structure of small cellular protrusions. In the example analyzed, for the first time the rod-like 3D structure of such a protrusion with a diameter of around 50 nm was elucidated by a far-field fluorescence microscopy approach. Such an almost ultra-structural 3D resolution would have been impossible to obtain by conventional confocal laser scanning fluorescence microscopy.

In the present report, only one type of molecules (fluorescent proteins localized in the cell membrane) was imaged by SPDM/SMI. For this, only one laser line was used for excitation, and the emission was limited to a small wavelength band. Thus, it should be possible to extend this method to appropriate multicolor SPDM/SMI imaging with several excitation wavelengths and appropriately discriminated emission spectra. In this case, however, chromatic aberrations have to be considered. Using high-quality objective lenses, these can still be as large as 50 nm in lateral (x, y) and 100 nm in axial (z) directions [37]. Therefore, special care has to be taken in multicolor SPDM/SALM imaging to correct for these aberrations by appropriate *in situ* calibration procedures [21, 26, 29, 36, 48, 49].

At the effective optical resolution levels of approx. 20 nm laterally and 50 nm axially reported here, numerous applications in the structural elucidation of cellular nanostructures are feasible. Examples for this are individual gene domains in the genetically active and inactive states; environmentally induced changes of chromatin nanostructure; size and nuclear distribution of replication factories and repair complexes; nuclear pore complex distribution; arrangement of polyribosomes; or the distribution of ion channels on the cell membrane. An additional important application will be the

possibility to count single molecules, e.g. on the cell membrane, or RNA transcripts. Although the SPDM procedure so far allows us to register only a part of all labeled molecules, the numbers obtained are minimum absolute numbers. For example, an SPDM count of 100 000 proteins in a cell membrane (upper plus lower membranes) of approximately $20\ \mu\text{m} \times 20\ \mu\text{m} \times 2 = 800\ \mu\text{m}^2$ would result in a minimum mean absolute membrane density of 125 proteins/ μm^2 , or 1 protein/8000 nm², or one protein in an area of 90 nm \times 90 nm. Furthermore, it would allow us to assess the homogeneity of molecule distribution at a resolution level in the macromolecular range. Numerous applications of such molecule counting and distribution analysis may be envisaged, from ‘fundamental molecular biophysics’ to the efficiency of pharmaceutical compounds’ transport across the cell membrane.

In case sufficiently photostable fluorochromes with photoconvertible ‘dark’ and ‘bright’ spectral signatures can be used, from the point of view of SPDM/SMI microscopy a further improvement of 3D effective resolution is anticipated. For example, if 5 000 to 10 000 photons could be registered from a single molecule, under otherwise ideal conditions an axial (z_0) localization accuracy of around 1 nm would be expected [50]. To achieve also a 1-nm lateral (x, y) localization accuracy with such photon numbers, in addition to axially structured illumination, laterally structured illumination [14, 53–55] might be used. Such an improvement in x, y, z localization would allow an effective optical 3D resolution in the 2-nm range, if the distance and orientation of the fluorophores are known. Hence, this would make possible far-field light optical structural analyses even of the components of macromolecular complexes in the interior of cells. Some possible examples might be: single gene domains; the replication factories responsible for the doubling of the cellular DNA; the repair complexes responsible for the repair of environmentally induced genome alterations; the chromatin remodeling/silencing complexes responsible for the expression-related modification of genome nanostructure; the transcription factories allowing the ‘reading’ of the genetic code; the splicing factories processing the transcribed RNA; the nuclear pore complexes controlling the traffic between cell nucleus and the rest of the cell; the ribosomes translating RNA into proteins; the proteasomes controlling the decomposition of proteins; the ion channel complexes controlling the transport of ions across the cell membrane; or the cell junction complexes responsible for formation of tissues.

To summarize, it is anticipated that SPDM/SALM and other novel developments in laser-optical nanoscopy will eventually bridge the gap in resolution between ultrastructural methods (nm resolution) and visible light far field microscopy (conventionally hundreds of nm resolution) in such a way that the same cellular structure can be imaged at

almost similar (down to molecular) resolution. Such a ‘correlative microscopy’ will provide an essential contribution to a direct insight into the ‘machinery’ of life on the individual cell level, from the change in folding of the chromatin fiber at the activation/silencing of a gene, to its transcription, to the processing of the mRNA produced, to the transport to the cytoplasm through the nuclear pores, to the translation into proteins, to the assembly and disassembly of macromolecular complexes, up to the signal transduction at the cell membrane and to cell-to-cell interactions. Beyond these exciting prospects for the molecular biophysics of the cell, it is anticipated that laser-optical nanoscopy methods will also provide an additional valuable tool for the analysis of the interaction of ‘biomolecular machines’ (BMMs) and pharmaceutical drugs on the level of single cells/single BMMs.

SPDM/SALM far field fluorescence microscopy approaches are expected to have highly relevant application perspectives not only in the biosciences and the physics of biological structures but also in the material sciences: for example, wherever a surface nanostructure has to be characterized, and fluorescence labeling of surface molecules is feasible, a fast light optical analysis would become possible and thus complement the higher resolution but also more time consuming elucidation by electron microscopy.

Acknowledgements We thank Dr. habil. Michael Wassenegger from AIPlanta in Neustadt/Weinstraße, Dr. Ingolf E. Blasig and Dr. Jörg Pirotek from the Leibniz Institute for Molecular Pharmacology (Berlin, Germany), Prof. Dr. Markus Sauer (Bielefeld University, Germany) for stimulating discussions concerning the use of physicochemically modified fluorescent proteins within biological specimens and supervision of the Ph.D. thesis of Manuel Gunkel and Dr. Victor Sourjik from ZMBH (University of Heidelberg) for further support.

We also thank Thomas Ruckelshausen, Christoph Hörmann, Heinz Eipel and Alexander Brunner (Kirchhoff Institute for Physics) for support of measurements and for stimulating discussions.

The financial support of the Deutsche Forschungsgemeinschaft (SPP1128) and of the European Union (Molecular Imaging Consortium) to Christoph Cremer, and of the Federal Ministry of Education and Research (BMBF) (services@MediGrid) to Michael Hausmann is gratefully acknowledged. Paul Lemmer is a fellow of the Excellence Cluster Cell Networks of the University of Heidelberg, and Thomas Ruckelshausen is a fellow of the Graduate Academy of Heidelberg University.

References

1. T. Cremer, C. Cremer, *Nat. Rev. Genet.* **2**, 292–301 (2001)
2. E.A. Jares-Erijman, T.M. Jovin, *Nat. Biotechnol.* **21**, 1387–1395 (2003)
3. J. Braga, J.M.P. Desterro, M. Carmo-Fonseca, *Mol. Biol. Cell* **15**, 4749–4760 (2004)
4. C. Cremer, T. Cremer, *Microsc. Acta* **81**, 31–44 (1978)
5. S.W. Hell, E.H.K. Stelzer, S. Lindek, C. Cremer, *Opt. Lett.* **19**, 222–224 (1994)
6. P.E. Hänninen, S.W. Hell, J. Salo, E. Soini, C. Cremer, *Appl. Phys. Lett.* **66**, 1698–1700 (1995)
7. A. Egner, S. Jakobs, S.W. Hell, *Proc. Natl. Acad. Sci. USA* **99**, 3370–3375 (2002)

8. J. Bewersdorf, B.T. Bennett, K.L. Knight, *Proc. Natl. Acad. USA* **103**, 18137–1814 (2006)
9. D. Baddeley, C. Carl, C. Cremer, *Appl. Opt.* **45**, 7056–7064 (2006)
10. B. Albrecht, A. Schweitzer, A.V. Failla, P. Edelmann, C. Cremer, *Appl. Opt.* **41**, 80–87 (2002)
11. A.V. Failla, A. Cavallo, C. Cremer, *Appl. Opt.* **4**, 6651–6659 (2002)
12. A.V. Failla, B. Albrecht, U. Spoeri, A. Kroll, C. Cremer, *Appl. Opt.* **41**, 7275–7283 (2002)
13. D. Baddeley, C. Batram, Y. Weiland, C. Cremer, U. Birk, *Nat. Protoc.* **2**, 2640–2646 (2007)
14. R. Heintzmann, T. Jovin, C. Cremer, *J. Opt. Soc. Am. A* **19**, 1599–1609 (2002)
15. S. Martin, A.V. Failla, U. Spöri, C. Cremer, A. Pombo, *Mol. Biol. Cell* **15**, 2449–2455 (2004)
16. G. Hildenbrand, A. Rapp, U. Spoeri, Ch. Wagner, C. Cremer, M. Hausmann, *Biophys. J.* **88**, 4312–4318 (2005)
17. H. Mathee, D. Baddeley, C. Wotzlaw, J. Fandrey, C. Cremer, U. Birk, *Histochem. Cell Biol.* **125**, 75–82 (2006)
18. G. Donnert, J. Keller, R. Medda, M.A. Andrei, S.O. Rizzoli, R. Lührmann, R. Jahn, C. Eggeling, S.W. Hell, *Proc. Natl. Acad. Sci. USA* **103**, 11440–11445 (2006)
19. S.W. Hell, I. Wichmann, *Opt. Lett.* **19**, 780–782 (1994)
20. M.A. Schwentker, H. Bock, M. Hofmann, S. Jakobs, J. Bewersdorf, C. Eggeling, S.W. Hell, *Microsc. Res. Tech.* **29**, 17262791 (2007)
21. H. Bornfleth, K. Sätzler, R. Eils, C. Cremer, *J. Microsc.* **189**, 118–136 (1998)
22. A.M. van Oijen, J. Köhler, J. Schmidt, G.J. Brakenhoff, *Chem. Phys. Lett.* **292**, 183–187 (1998)
23. T.D. Lacoste, X. Michalet, F. Pinaud, D.S. Chemla, A.P. Alivisatos, S. Weiss, *Proc. Natl. Acad. Sci. USA* **97**, 9461–9466 (2000)
24. M. Schmidt, M. Nagorni, S.W. Hell, *Rev. Sci. Instrum.* **71**, 2742–2745 (2000)
25. C. Cremer, A.V. Failla, B. Albrecht, US Patent 7,298,461 B2, filed 9 Oct. 2001
26. M. Heilemann, D.P. Herten, R. Heintzmann, C. Cremer, C. Müller, Ph. Tinnefeld, K.D. Weston, J. Wolfrum, *Anal. Chem.* **74**, 3511–3517 (2002)
27. C. Cremer, M. Hausmann, J. Bradl, B. Rinke, German Patent Application No. 196.54. 824.1/DE, filed 23 Dec. 23 1996; European Patent EP 1997953660, 8 Apr. 1999; Japanese Patent JP 1998528237, 23 June 1999; United States Patent US 09331644, 25 Aug. 1999
28. C. Cremer, P. Edelmann, H. Bornfleth, G. Kreth, H. Muench, H. Luz, M. Hausmann, in *Handbook of Computer Vision and Applications*, vol. 3 ed. by B. Jähne, H. Haußecker, P. Geißler (Academic Press, San Diego, 1999), pp. 839–885
29. A. Esa, P. Edelmann, L. Trakthenbrot, N. Amariglio, G. Rechavi, M. Hausmann, C. Cremer, *J. Microsc.* **199**, 96–105 (2000)
30. E. Betzig, G.H. Patterson, R. Sougrat, O.W. Lindwasser, S. Olenych, J.S. Bonifacino, M.W. Davidson, J. Lippincott-Schwartz, H.F. Hess, *Scienceexpress* **313**, 1642–1645 (2006)
31. S.T. Hess, T.P.K. Girirajan, M.D. Mason, *Biophys. J.* **91**, 4258–4272 (2006)
32. M. Bates, B. Huang, G.T. Dempsey, X. Zhuang, *Science* **317**, 1749–1753 (2007)
33. C. Geisler, A. Schönle, C. von Middendorf, H. Bock, C. Eggeling, A. Egner, S.W. Hell, *Appl. Phys. A* **88**, 223–226 (2007)
34. B. Huang, W. Wang, M. Bates, X. Zhuang, *Science* **319**, 810–813 (2008)
35. A.K. Lidke, B. Rieger, T.M. Jovin, R. Heintzmann, *Opt. Express* **13**, 7052–7062 (2005)
36. A. Esa, A.E. Coleman, P. Edelmann, S. Silva, C. Cremer, S. Janz, *Cancer Genet. Cytogenet.* **127**, 168–173 (2001)
37. J. Rauch, T.A. Knoch, I. Solovei, K. Teller, S. Stein, K. Buiting, B. Horsthemke, J. Langowski, T. Cremer, M. Hausmann, C. Cremer, *Differentiation* **76**, 66–82 (2008)
38. T.B. McAnaney, W. Zeng, C.F.E. Doe, N. Bhanji, S. Wakelin, D.S. Pearson, P. Abbyad, X. Shi, S.G. Boxer, C.R. Bagshaw, *Biochemistry* **44**, 5510–5524 (2005)
39. C. Eggeling, J. Widengren, R. Rigler, C.A.M. Seidel, *Anal. Chem.* **70**, 2651–2659 (1998)
40. J. Lippincott-Schwartz, N. Altan-Bonnet, G.H. Patterson, *Nat. Biotechnol.* **20**, 87–90 (2002)
41. R.Y. Tsien, *Ann. Rev. Biochem.* **67**, 509–544 (1998)
42. T. Nagai, K. Ibata, E.S. Park, M. Kubota, K. Mikoshiba, A. Miyawaki, *Genetics* **122**, 19–27 (1989)
43. M. Schmidt, M. Nagorni, S.W. Hell, *Rev. Sci. Instrum.* **71**, 2742–2745 (2000)
44. J. Enderlein, E. Toprak, P.R. Selvin, *Opt. Express* **14**, 8111–8120 (2006)
45. F. Aguet, D. Van De Ville, M. Unser, *Opt. Express* **13**, 10503–10522 (2005)
46. M.F. Juette, T.J. Gould, M.D. Lessard, M.J. Mlodzianoski, B.S. Nagpure, B.T. Bennett, S.T. Hess, J. Bewersdorf, *Nat. Methods* (2008)
47. J. Reymann, D. Baddeley, P. Lemmer, W. Stadter, T. Jegou, K. Rippe, C. Cremer, U. Birk, *Chromosome Res.* **16**, 367–382 (2008)
48. P. Edelmann, C. Cremer, *Proc. SPIE* **3921**, 313–320 (2000)
49. S. Fenz, S.H. Mathee, G. Kreth, D. Baddeley, Y. Weiland, J. Schwarz-Finsterle, C.G. Cremer, U.J. Birk, *Proc. SPIE* **6630**, 663002-1 (2007)
50. B. Albrecht, A.V. Failla, R. Heintzmann, C. Cremer, *J. Biomed. Opt.* **6**, 292–299 (2001)
51. D.H. Burns, J.B. Callis, G.D. Christian, E.R. Davidson, *Appl. Opt.* **24**, 154–161 (1985)
52. E. Betzig, *Opt. Lett.* **20**, 237–239 (1995)
53. R. Heintzmann, C. Cremer, *Proc. SPIE* **3658**, 185–195 (1999)
54. J.T. Frohn, H.F. Knapp, A. Stemmer, *Proc. Natl. Acad. Sci. USA* **97**, 7232–7236 (2000)
55. M. Gustafsson, L. Shao, P.M. Carlton, C.J.R. Wang, I.N. Golubovskaya, W.Z. Cande, D.A. Agard, J.W. Sedat, *Biophys. J.*, 13 March (2008)